Downlink Transmission in RIS-enhanced Cell-Free Network: Analysis and Optimization

Xuanhong Yan, Taotao Ji, *Graduate Student Member, IEEE,* Zheng Wang, *Senior Member, IEEE,* Yongming Huang, *Senior Member, IEEE*

***Abstract*—This letter examines the performance of RIS-enhanced cell-free network (RIS-CFN) with multiple user groups under different transmission modes, subject to fronthaul capacity constraints. It derives the SINR under both coherent and non-coherent transmission modes. Unlike coherent transmission, non-coherent transmission is unaffected by asynchronous reception. An adequate number of access points (APs) can meet the data rate requirements of user equipment (UE). Based on these insights, an iterative joint power allocation and passive beamforming algorithm (JPAPB) is developed for non-coherent transmission, considering selecting partial APs for UE and fronthaul capacity limit. Simulations show that non-coherent transmission with JPAPB outperforms coherent transmission under limited fronthaul capacity. Experimental results also validate JPAPB's effectiveness and the performance gains from RIS.**

***Index Terms*—Downlink reconfigurable intelligent surface-enhanced cell-free network, power allocation, passive beamforming design**

I. Introduction

Reconfigurable intelligent surface (RIS) is a revolutionary technology that smartly modifies the wireless environment by altering the phase shift and amplitude of its passive elements [1]. It has the advantages of easy deployment, low power, and low cost. Due to these advantages, RIS has been applied in various scenarios, for example, RIS-assisted satellite communication [2], [3], RIS-assisted cell-free network (RIS-CFN) [4]–[7]. Notably, researchers in [4] introduced the technology of simultaneously transmitting and reflecting RIS (STAR-RIS) for providing for UEs in front and behind the surface. The authors investigated the uplink&downlink spectral efficiency in the spatially correlated RIS-CFN [5], [6]. [7] also highlighted the joint design of active and passive beamforming to enhance data rate performance in RIS-assisted systems.

However, the analysis of asynchronous reception under the coherent transmission mode on system performance was limited in only CFN so far [8]–[10], which has not yet been considered in the RIS-CFN scenario. Additionally, in multi-AP systems, the fronthaul link may face significant capacity pressure under coherent transmission, an important aspect that has not been thoroughly discussed for RIS-CFN in [11], [12].

Against the above background, this study compares data rate in downlink RIS-CFN under coherent and non-coherent transmission modes. Key contributions include deriving data rate lower bounds for both modes with statistical CSI and fronthaul capacity constraints and analyzing the impact of AP numbers. Additionally, a joint power allocation and passive beamforming design algorithm (JPAPB) is proposed. Experimental results show the JPAPB enhances data rate performance under non-coherent transmission more effectively than under coherent transmission when facing capacity constraints.

This work was supported by the National Natural Science Foundation of China under Grant 62225107 and Grant 62371124, the Fundamental Research Funds for the Central Universities under Grant 2242022k60002, the Natural Science Foundation on Frontier Leading Technology Basic Research Project of Jiangsu under Grant BK20222001.

X. Yan, T. Ji, Z. Wang, and Y. Huang are with the School of Information Science and Engineering, the National Mobile Communications Research Laboratory, Southeast University, Nanjing 210096, China, and also with the Pervasive Communications Center, Purple MountainLaboratories, Nanjing 211111, China (e-mail: {yanxuanhong, jitaotao, huangym}@seu.edu.cn, wznuaa@gmail.com)

II. System model

As shown in Fig. 1, a time division duplex (TDD) downlink RIS-CFN is considered, including one RIS, K APs, and M UEs. Each RIS has N elements, each AP has N_t antennas, and each UE has $N_r = 1$ antennas. The RIS and APs are connected to a central processing unit (CPU), which is responsible for the joint transmission. A more realistic channel model is adopted, where the spatial correlation between the RIS elements is taken into account [4]. The RIS-CFN channel model consists of three kinds of channels: the direct AP-UE channel $\hat{\mathbf{h}}_{mk}$, the AP-RIS channel $\mathbf{G}_k$ and the RIS-UE channel $\mathbf{v}_m$. Specifically, $\hat{\mathbf{h}}_{mk} = \sqrt{\beta_{mk}}\hat{\mathbf{R}}_{mk}^{\frac{1}{2}}\mathbf{a}_{mk}$, $\mathbf{G}_k = \sqrt{\gamma_m}\mathbf{R}_{\mathrm{RIS},k}^{\frac{1}{2}}\mathbf{D}_k\mathbf{R}_{\mathrm{AP},k}^{\frac{1}{2}}$, and $\mathbf{v}_m = \sqrt{\alpha_m}\mathbf{R}_{\mathrm{RIS},m}^{\frac{1}{2}}\mathbf{c}_m$. $\mathbf{R}_{\mathrm{RIS},k} \in \mathbb{C}^{N\times N}$, $\mathbf{R}_{\mathrm{AP},k} \in \mathbb{C}^{N_t\times N_t}$, and $\mathbf{R}_{\mathrm{RIS},m} \in \mathbb{C}^{N\times N}$ denote the deterministic Hermitian-symmetric positive semidefinite correlation matrices at the RIS and the AP, which are assumed to be known. Also, $\hat{\mathbf{R}}_{mk} \in \mathbb{C}^{N_t\times N_t}$ denotes the channel covariance matrice. Also, $\{\beta_{mk}, \gamma_k, \alpha_m\}$ denote the large-scale fading. $\mathbf{a}_{mk} \sim \mathcal{CN}(0, \mathbf{I}_{N_t})$, $\mathbf{c}_m \sim \mathcal{CN}(0, \mathbf{I}_N)$, $\mathbf{D}_k \sim \mathcal{CN}(0, \mathbf{I}_{NN_t})$ are the corresponding fast-fading vectors. Therefore, the equivalent baseband channel from k-th AP to m-th UE is modeled as

$$\mathbf{h}_{mk} = \underbrace{\hat{\mathbf{h}}_{mk}}_{\text{direct}} + \underbrace{\mathbf{v}_m\mathbf{\Phi}\mathbf{G}_k}_{\text{reflection}} = \hat{\mathbf{h}}_{mk} + \underbrace{\boldsymbol{\theta}\mathrm{diag}\left(\mathbf{v}_m\right)\mathbf{G}_k}_{\mathbf{g}_{mk}}, \tag{1}$$

where $\mathbf{\Phi} = \mathrm{diag}\left(\phi_1, \ldots, \phi_N\right) \in \mathbb{C}^{N\times N}$ denotes the phase-shift matrix of RIS. By introducing an auxiliary vector $\boldsymbol{\theta}$ with $\theta_i = \left(\phi_i\right)^*, \forall i$, the reformed phase-shift vector is expressed as $\boldsymbol{\theta}^{\mathrm{H}} = [\theta_1, \ldots, \theta_i, \ldots] \in \mathbb{C}^{1\times N}$, where $|\theta_i| = 1$.

Let $\mathcal{K}_m$ be the serving AP set of m-th UE and $\mathbf{w}_{mk} \in \mathbb{C}^{N_r\times N_t}$ be the beamforming vector from k-th AP to m-th

TABLE I
COMPARISON OF THE DOWNLINK SINR UNDER COHERENT AND NON-COHERENT RIS-CFN

Downlink SINR	**Coherent Transmission Strategy**	**Non-coherent Transmission Strategy**
Useful signal Power DSP_m	$\left\lvert \sum_{k\in\mathcal{K}_m} \sqrt{p_{mk}} \left(\theta_{mk}^{(d)} \mathbb{E}\left\{\hat{\mathbf{h}}_{mk}^{\mathrm{H}} \hat{\mathbf{h}}_{mk}\right\} + \theta_{mk}^{(r)} \mathbb{E}\left\{\mathbf{g}_{mk}^{\mathrm{H}} \mathbf{g}_{mk}\right\}\right) \right\rvert^2$	$\sum_{k\in\mathcal{K}_m} p_{mk} \left\lvert \left(\mathbb{E}\left\{\hat{\mathbf{h}}_{mk}^{\mathrm{H}} \hat{\mathbf{h}}_{mk}\right\} + \mathbb{E}\left\{\mathbf{g}_{mk}^{\mathrm{H}} \mathbf{g}_{mk}\right\}\right) \right\rvert^2$
Interference Power INT_m	$\sum_{n=1} \sum_{j\in\mathcal{K}_n} p_{nj} \mathrm{Tr}\left(\mathbf{R}_{mj} \mathbf{R}_{\mathbf{nj}}\right) - \mathrm{DSP}_m$	$\sum_{n\neq m} \sum_{j\in\mathcal{K}_n} p_{nj} \mathrm{Tr}\left(\mathbf{R}_{mj} \mathbf{R}_{nj}\right)$
Fronthual Capacity for k-th AP	$\sum \mathbb{I}\left(p_{mk}\right) \log_2\left(1 + \frac{\mathrm{DSP}_m}{\mathrm{INT}_m + \sigma_m^2}\right) \leq C_k$	$\sum \mathbb{I}\left(p_{mk}\right) R_{mk} \leq C_k$

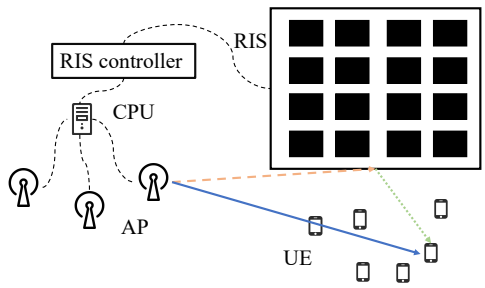

Fig. 1. A RIS enhanced cell-free network.

UE. Thus, the received signal at UE m is denoted as

$$\mathbf{y}_m = \underbrace{\sum_{k\in\mathcal{K}_m} \mathbf{h}_{mk} \mathbf{w}_{mk}^{\mathrm{H}} \mathbf{x}_{mk}}_{\text{desired signal}} + \underbrace{\sum_{n\neq m} \sum_{j\in\mathcal{K}_n} \mathbf{h}_{mj} \mathbf{w}_{nj}^{\mathrm{H}} \mathbf{x}_{nj}}_{\text{interference}} + \underbrace{\mathbf{n}_m}_{\text{noise}}, \tag{2}$$

where $\mathbb{E}\left\{\mathbf{x}_{mk} \mathbf{x}_{mk}^{\mathrm{H}}\right\} = 1$ and $\mathbb{E}\left\{\mathbf{n}_m \mathbf{n}_m^{\mathrm{H}}\right\} = \sigma_m^2$ are respectively the baseband signal and additive white Gaussian noise (AWGN).

III. Data Rate Performance Analysis

This section analyzes the impact of asynchronous transmission on the RIS-CFN system. It then derives and analyzes closed-form data rate expressions for coherent and non-coherent transmission modes, using the use-and-then-forget (UatF) rate and conjugate beamforming (CB) scheme.

1) Coherent Transmission: First, we analyze asynchronous reception in RIS-CFN with coherent transmission, focusing on two link types: direct (d) and reflected (r). Asynchronous signal arrival is caused by the varying distances between APs and a given UE due to different AP locations in the CFN, introducing a constant phase shift:

$$\theta_{mk}^{(x)} = e^{-j2\pi \frac{\Delta t_{mk}^{(x)}}{T_s}}, x \in \{d, r\} \tag{3}$$

where $\Delta t_{mk}^{(x)} = \Delta d_{mkj}^{(x)} / c$ represents the timing offset for the signal intended for the m-th UE and transmitted by the k-th AP. $\Delta d_{mkj}^{(x)}$, c, and T_s are the propagation delay, speed of light, and symbol duration, respectively. Assuming the first arrived signal to UE m is from AP j and its timing offset is $\Delta t_{mj}^{(x)} = 0$, the equivalent channel between the m-th UE and the k-th AP under asynchronous reception is rewritten as

$$\mathbf{h}_{mk}^{\mathrm{Asy}} = \theta_{mk}^{(d)} \hat{\mathbf{h}}_{mk} + \theta_{mk}^{(r)} \mathbf{g}_{mk}. \tag{4}$$

According to the study by [5], the downlink data rate for coherent transmission in RIS-CFN, not accounting for channel estimation errors, is summarized in Tab. I.

2) Non-Coherent Transmission: Then, we give the analysis of the downlink performance in RIS-CFN under non-coherent transmission.

Lemma 1 (The lower bound of data rate): For the downlink non-coherent RIS-CFN system, the lower bound of the data rate R_m can be expressed as

$$R_m = \log_2\left(1 + \mathrm{SINR}_m^{\mathrm{U}}\right), \tag{5}$$

where

$$\mathrm{SINR}_m = \frac{\mathrm{DSP}_m}{\mathrm{INT}_m + \sigma_m^2}, \tag{6}$$

$$\mathrm{DSP}_m = \sum_{k\in\mathcal{K}_m} \left(\mathrm{Tr}\left(\mathbf{R}_{mk}\right)\right)^2 p_{mk}, \tag{7}$$

$$\mathrm{INT}_m = \sum_{n\neq m} \sum_{j\in\mathcal{K}_n} \mathrm{Tr}\left(\mathbf{R}_{mj} \mathbf{R}_{nj}\right) p_{nj}. \tag{8}$$

DSP_m and INT_m denotes the desired signal power of m-th UE and the interference power of m-th UE, respectively. Also, $\mathbf{R}_{mk} = \mathbb{E}\left\{\mathbf{h}_{mk}^{\mathrm{H}} \mathbf{h}_{mk}\right\}$.

Proof: In non-coherent transmission, UE m decodes the signals one by one from all related APs. Then, the received signal at UE m is rewritten as

$$\begin{aligned} \mathbf{y}_m =& \mathbf{h}_{mk} \mathbf{w}_{mk}^{\mathrm{H}} \mathbf{x}_{mk} + \sum_{j>k, j\in\mathcal{K}_m} \mathbf{h}_{mj} \mathbf{w}_{mj}^{\mathrm{H}} \mathbf{x}_{mj} \\ &+ \sum_{n\neq m} \sum_{j\in\mathcal{K}_n} \mathbf{h}_{mj} \mathbf{w}_{nj}^{\mathrm{H}} \mathbf{x}_{nj} + \mathbf{n}_m. \end{aligned} \tag{9}$$

With the same operation as [Eq (8) - Eq (14)] in [12], the data rate lower bound is derived as,

$$R_{mk} = \log_2\left(1 + \frac{p_{mk} \left\lvert \mathbb{E}\left\{\mathbf{h}_{mk}^{\mathrm{H}} \mathbf{h}_{mk}\right\} \right\rvert^2}{\mathrm{SI}_m + \mathrm{INT}_m + \sigma_m^2}\right), \tag{10}$$

where $\mathrm{SI}_m = \sum_{j>k, j\in\mathcal{K}_m} \mathrm{Tr}\left(\left(\mathbf{R}_{mj}\right)\right)^2 p_{mj}$. According to [10], [12], the total achievable data rate for UE m can be derived by computing $R_m = \sum_{k\in\mathcal{K}_m} R_{mk}$. ■

The downlink SINR for non-coherent transmission in RIS-CFN is also summarized in Tab. I. This table shows that under coherent transmission, asynchronous reception more significantly affects the useful signal power in RIS-CFN compared to pure CFN, where only the direct link is affected. In RIS-CFN, both direct and reflected links are subject to asynchronous effects. In contrast, under non-coherent transmission, both the direct and reflected links are not influenced by asynchronous reception. Additionally, coherent transmission is more prone to reaching the fronthaul link capacity limit than non-coherent transmission.

From Lemma 1, the data rate is related to the statistical CSI from APs to UEs, the related serving AP set $\mathcal{K}_m$, phase shifts $\boldsymbol{\theta}$, and the transmitting power p_{mk}. Next, we will illustrate through Corollary 1 that a finite number of APs can ensure relatively satisfactory data rate performance for the RIS-CFN system.

Corollary 1: When $K \to +\infty$, the data rate of the m-th UE is upper bounded.

Proof: For simplicity, we assume there is no inter-group interference in the system and assume the phase shifts of RIS to be random. The data rate of m-UE is expressed as,

$$R_m = \mathbb{E}\left\{\log_2\left(1+\frac{\sum_{k\in\mathcal{K}}\mathbf{D}_{mk}^{\mathrm{H}}\mathbf{D}_{mk}}{\sum_{k\in\mathcal{K}}\boldsymbol{\Psi}_{mk}+\sigma_m^2}\right)\right\}, \tag{11}$$

where

$$\begin{aligned}\mathbf{D}_{mk} &= \mathbb{E}\left\{p_{mk}^{1/2}\left(\left\|\hat{\mathbf{h}}_{mk}\right\|^2+\left\|\mathbf{g}_{mk}\right\|^2\right)\right\} \qquad (12)\\ &= p_{mk}^{1/2}N_t\left(\beta_{mk}+N\alpha_m\gamma_k\right),\\ \boldsymbol{\Psi}_{mk} &= \mathbb{E}\left\{\sum_{n\neq m}^{M}p_{nj}\mathbf{h}_{mk}\mathbf{h}_{nj}^{\mathrm{H}}\mathbf{h}_{nj}\mathbf{h}_{mk}^{\mathrm{H}}+\sigma_m^2\right\} \qquad (13)\\ &= \sum_{n\neq m}^{M}p_{nj}N_t\left(\beta_{mj}+N\alpha_m\gamma_j\right)\left(\beta_{nj}+N\alpha_n\gamma_j\right).\end{aligned}$$

Let $A=\sum_{k\in\mathcal{K}}\mathbf{D}_{mk}^{\mathrm{H}}\mathbf{D}_{mk}$, $B=\sum_{k\in\mathcal{K}}\boldsymbol{\Psi}_{mm}+\sigma_m^2$, $x_K=\mathbf{D}_{mK}^{\mathrm{H}}\mathbf{D}_{mK}$ and $y_K=\boldsymbol{\Psi}_{mK}$. Assuming the $K-1$-th, K-th, and $K+1$-th APs are co-located, $x_{K-1}=x_K=x_{K+1}$ and $y_{K-1}=y_K=y_{K+1}$ hold. APs are ranked by $\frac{x_1}{y_1}>\frac{x_2}{y_2}>\cdots>\frac{x_{K-1}}{y_{K-1}}$. This assumption is reasonable because as the number of APs increases, the path loss from newly added APs to the current UE also increases, leading to a decrease in the newly added received power. If the data rate is bounded as the increasing K, then R_m must satisfy

$$R_m^K-R_m^{K-1}>R_m^{K+1}-R_m^K, \tag{14}$$

where R_m^K is the data rate for m-th UE with K APs. That is,

$$\begin{aligned}&\frac{A}{B}-\frac{A-x_K}{B-y_K}>\frac{A+x_K}{B+y_K}-\frac{A}{B}\\ &\frac{1}{B\left(B-y_K\right)}\overset{(a)}{>}\frac{1}{B\left(B+y_K\right)}.\end{aligned} \tag{15}$$

(a) holds as $\frac{x_1}{y_1}>\cdots>\frac{x_{K-1}}{y_{K-1}}$ holds. The above derivation proves that (14) holds. Hence, the proof is completed. ■

Corollary 1 indicates that the gain from increasing the number of APs is limited and that a moderate number of APs is sufficient to satisfy UEs data rate requirements.

IV. The Proposed JPAPB Algorithm

In this section, we study the joint optimization of power allocation and phase shifts, aiming to maximize the weighted lower bound of the data rate in RIS-CFN. Additionally, it is essential to consider the fronthaul capacity limit, which can be expressed as follows:

$$\sum\mathbb{I}\left(p_{mk}\right)R_{mk}\leq C_k,\forall k, \tag{16}$$

where C_k is the fronthual capacity limit and $\mathbb{I}\left(p_{mk}\right)$ is the indicator function. If $p_{mk}\neq 0$, $\mathbb{I}\left(p_{mk}\right)=1$; $p_{mk}=0$, otherwise.

Given the derived result in Lemma 1, the problem can be formally formulated as

$$\begin{aligned}(\mathrm{P0})\quad \max_{\{\mathbf{p},\Theta\}}\quad & \sum_m\delta_m R_m,\\ \text{s.t.}\quad & (16),\\ & \sum_m p_{mk}\leq \mathrm{P}_{\max},\ \forall k\in\mathcal{K}, \qquad (17a)\\ & |\theta_i|=1,\forall i\in\mathcal{N}, \qquad (17b)\end{aligned}$$

where $\mathrm{P}_{\max}$ is the maximum transmitting power of each AP. Without loss of generality, we consider the prior weight δ_m of the m-th UE. Leveraging Corollary 1, we assume a moderate number of APs serving one UE by introducing an indicator, s_{mk}. If $s_{mk}=1$, m-th UE is served by k-th AP; $s_{mk}=0$, otherwise. Here, we determine the AP set for one UE according to large-scale fading. Principally, (P0) is challenging to solve because it is NP-hard.

A. Power Allocation: Solving for $\mathbf{p}$ with fixed Θ

In [13], Lagrangian dual transform is introduced to convert the sum logarithm structure into the sum of ratio form $f_{\boldsymbol{\gamma}}\left(\boldsymbol{\gamma},\mathbf{p},\boldsymbol{\theta}\right)$, by introducing multipliers $\boldsymbol{\gamma}=\{\gamma_m\},\forall m$,

$$f_{\boldsymbol{\gamma}}=\sum_m\mathcal{C}_m+\frac{\delta_m\left(1+\gamma_m\right)\mathcal{A}_m}{\mathcal{B}_m-\mathcal{A}_m+\sigma^2}, \tag{18}$$

where $\mathcal{A}_m=\sum_{k\in\mathcal{K}_m}\left(\mathrm{Tr}\left(\mathbf{R}_{mk}\right)\right)^2p_{mk}$, $\mathcal{B}_m=\sum_n\sum_{j\in\mathcal{K}_n}\mathrm{Tr}\left(\mathbf{R}_{mj}\mathbf{R}_{nj}\right)p_{nj}$ and $\mathcal{C}_m=\delta_m\left[\log_2(1+\gamma_m)-\gamma_m\right]$. $f_{\boldsymbol{\gamma}}$ is convex about γ_m with given $\{\mathbf{p},\boldsymbol{\theta}\}$. The optimal $\gamma_m^*=\mathrm{SINR}_m$ can be obtained by solving $\partial f_{\boldsymbol{\gamma}}/\partial\gamma_m=0$. To optimize the left variables $\{\mathbf{p},\boldsymbol{\theta}\}$ with a given γ_m, (18) is reconstructed into a non-ratio form according to the multi-dimensional quadratic transform in [13], namely,

$$f_q=\sum_m\mathcal{C}_m+f_{\mathbf{y}}\left(\boldsymbol{\gamma},\mathbf{p},\boldsymbol{\theta},\mathbf{y}\right) \tag{19}$$

with

$$\begin{aligned}f_{\mathbf{y}}=&2\sum_m\sqrt{\delta_m(1+\gamma_m)}\sum_{k\in\mathcal{M}_m}y_{mk}\mathrm{Tr}\left(\mathbf{R}_{mk}\right)\sqrt{p_{mk}}\\ &-\sum_m\sum_{k\in\mathcal{K}_m}y_{mk}^2\left(\sigma_m^2+\mathcal{B}_m\right).\end{aligned} \tag{20}$$

Here, an auxiliary variable y_{mk} is introduced with respect to each pair, while the collection of auxiliary variable $\{y_{mk}\}$ is denoted by $\mathbf{Y}$. Given $\{\boldsymbol{\gamma},\mathbf{p},\boldsymbol{\theta}\}$ in the new objective function f_q, $\mathbf{Y}$ can be determined via solving $\partial f_q/\partial y_{mk}=0$. Therefore, the optimal y_{mk} is

$$y_{mk}^*=\left(\sigma^2+\mathcal{B}_m\right)^{-1}\kappa_m\mathrm{Tr}\left(\mathbf{R}_{mk}\right)\sqrt{p_{mk}} \tag{21}$$

with $\kappa_m=\sqrt{\delta_m(1+\gamma_m)}$.

After determining $\{\boldsymbol{\gamma},\mathbf{y}\}$, $\mathbf{p}$ and $\boldsymbol{\theta}$ remain to be solved. The rest problem with fixed $\boldsymbol{\theta}$ is still difficult to solve as the indicator function and the real-time data rate R_{mk}. The indicator function in (16) can be equivalently expressed as an l_0-norm of a scalar, which can be approximated as a convex

reweighted l_1-norm form. To deal with real-time data rate, we replace R_{mk} with $\hat{R}_{mk}$ obtained from the previous iteration. Specifically, the constraint (16) can be rewritten as

$$\sum_m \alpha_{mk} p_{mk} \hat{R}_{mk} \leq C_k, \tag{22}$$

where $\alpha_{mk} = \frac{1}{p_{mk}+\epsilon}$ and ϵ is a small constant regularization parameter, preventing α_{mk} from being infinity. The problem (P0) is reformulated as

$$\begin{aligned} (\text{P1}) \quad & \max_{\{\mathbf{p}\}} \quad f_{\mathbf{y}}, \\ & \text{s.t.} \quad (17a), (22), \end{aligned} \tag{23a}$$

With fixed α_{mk} and $\hat{R}_{mk}$, (P1) about $\mathbf{p}$ is a classic convex quadratic optimization problem, which can be solved by CVX.

B. Passive Beamforming: Solving for Θ with fixed $\mathbf{p}$

With the fixed $\{\boldsymbol{\gamma}, \mathbf{p}\}$, the new objective function for the remaining optimization problem is transformed from (18) to

$$f_p = \sum_m \mathcal{C}_m + f_{\boldsymbol{\beta}}(\boldsymbol{\gamma}, \mathbf{p}, \boldsymbol{\theta}, \boldsymbol{\beta}) \tag{24}$$

with

$$\begin{aligned} f_{\boldsymbol{\beta}} =& 2 \sum_m \sqrt{\delta_m (1+\gamma_m)} \sum_{k \in \mathcal{K}_m} \beta_{mk} \mathrm{Tr}\left(\mathbf{R}_{mk}\right) \sqrt{p_{mk}} \\ & - \sum_m \sum_{k \in \mathcal{K}_m} \beta_{mk}^2 \left(\sigma_m^2 + \mathcal{B}_m\right). \end{aligned} \tag{25}$$

Clearly, this computation for β_{mk}^* is similar to the computation for $\mathbf{y}_{mk}^*$,

$$\beta_{mk}^* = \left(\sigma_m^2 + \mathcal{B}_m\right)^{-1} \kappa_m \mathrm{Tr}\left(\mathbf{R}_{mk}\right) \sqrt{p_{mk}}. \tag{26}$$

Denote $\mathbf{w} = \boldsymbol{\theta}^{\mathrm{H}} \boldsymbol{\theta} \succeq \mathbf{0}_N$, $\mathbf{A}_{mk} = \mathrm{diag}\left(\mathbf{v}_m\right) \mathbf{G}_k$, f_{p} is rewritten as

$$f_{\mathrm{new}} = - \sum_m \sum_k \beta_{mk}^2 U_{\mathbf{w},mk} + \mathrm{Tr}\left(\boldsymbol{\nu} \mathbf{w}\right) + C, \tag{27}$$

where

$$U_{\mathbf{w},mk} = \sum_n \sum_j p_{nj} \mathrm{Tr}\left(\mathbf{w}^{\mathrm{H}} \mathbf{A}_{nj}^{\mathrm{H}} \mathbf{A}_{mj}^{\mathrm{H}} \mathbf{w} \mathbf{A}_{mj} \mathbf{A}_{nj}^{\mathrm{H}}\right), \tag{28a}$$

$$\begin{aligned} \boldsymbol{\nu} = & \sum_m \sum_{k \in \mathcal{K}_m} [2\kappa_m \beta_{mk} \sqrt{p_{mk}} \mathbf{A}_{mk} \mathbf{R} A_{mk}^H - \beta_{mk}^2 \\ & \sum_n \sum_{j \in \mathcal{K}_n} p_{nj} \left(\mathbf{A}_{mj} \hat{\mathbf{R}}_{nj} \mathbf{A}_{mj}^H + \mathbf{A}_{nj} \hat{\mathbf{R}}_{mj} \mathbf{A}_{nj}^H\right)], \end{aligned} \tag{28b}$$

$$\begin{aligned} C = & \sum_m \sum_{k \in \mathcal{K}_m} [2\kappa_m \beta_{mk}^{\mathrm{H}} \sqrt{p_{mk}} \mathrm{Tr}\left(\hat{\mathbf{R}}_{mk}\right) - \\ & |\beta_{mk}|^2 \sum_n \sum_{j \in \mathcal{K}_n} p_{nj} + \sigma_m^2]. \end{aligned} \tag{28c}$$

Then, the reformulated subproblem about $\boldsymbol{\theta}$ is reduced to

$$\begin{aligned} (\text{P2}) \quad & \min_{\{\mathbf{w}\}} \quad \sum_m \sum_k \beta_{mk}^2 U_{\mathbf{w},mk} - \mathrm{Tr}\left(\boldsymbol{\nu} \mathbf{w}\right), \\ & \text{s.t.} \quad \mathbf{w} \succeq \mathbf{0}_N, \mathbf{w}_{n,n} = 1. \end{aligned} \tag{29a}$$

Problem (P2) is a standard convex semidefinite program (SDP). Hence, it can be solved by existing convex optimization solvers such as CVX. However, $\mathbf{w}$ can not meet the rank-one constraint $\mathrm{Rank}\left(\mathbf{w}\right) = 1$, which is non-convex and relaxed to $\mathbf{w}_{n,n} = 1$ in (P2). Consequently, an additional step is required to construct a suboptimal rank-one solution from $\mathbf{w}$.

Algorithm 1 The Proposed JPAPB Algorithm

Initialization: Initialize $\mathbf{w}_{mk}$, $\boldsymbol{\theta}$ and maximum iteration number T.

while $t \leq T$ **do**
  Update $\boldsymbol{\gamma}^{(t)}$ with $\mathbf{p}^{(t-1)}$ and $\boldsymbol{\theta}^{(t-1)}$,
  Update $\mathbf{y}^{(t)}$ by (21) with $\mathbf{p}^{(t-1)}$, $\boldsymbol{\gamma}^{(t)}$, and $\boldsymbol{\theta}^{(t-1)}$,
  Update $\mathbf{p}^{(t)}$ by solving (P1) with $\boldsymbol{\gamma}^{(t)}$, $\mathbf{y}^{(t)}$, and $\boldsymbol{\theta}^{(t-1)}$,
  Update $\boldsymbol{\beta}^{(t)}$ by (26) with $\mathbf{p}^{(t)}$ and $\boldsymbol{\gamma}^{(t)}$,
  Update $\boldsymbol{\theta}^{(t)}$ by solving (P2) with $\boldsymbol{\gamma}^{(t)}$, $\boldsymbol{\beta}^{(t)}$, and $\mathbf{p}^{(t)}$,
  Compute α_{mk} and $\hat{R}_{mk}$ with $\mathbf{p}^{(t)}$ and $\boldsymbol{\theta}^{(t)}$,
  $t = t + 1$,
end while

First, we obtain the eigenvalue decomposition of $\mathbf{w}$ as $\mathbf{w} = \mathbf{U} \sum \mathbf{U}$, where $\mathbf{U} = [e_1, \ldots, e_N]$ and $\sum = \mathrm{diag}\left(\lambda_1, \ldots, \lambda_N\right)$ are a unitary matrix and a diagonal matrix, respectively. Second, we compute $\boldsymbol{\theta} = \mathbf{U} \sum^{1/2} \mathbf{r}$, where $\mathbf{r}$ is a random vector generated with $\mathcal{CN} \sim (0, \mathbf{I}_N)$ denoting the circularly symmetric complex Gaussian (CSCG) distribution. With independently generated Gaussian random vectors $\mathbf{r}$, the objective value of (P2) is approximated as the minimum one attained by the best $\boldsymbol{\theta}$ among all $\mathbf{r}$.

V. Simulations

In this section, Monte Carlo simulations corroborate the proposed JPAPB algorithm's performance. The network settings mainly refer to [7]. The RIS and APs are located at $(60, 10, 6)$m and $(40k, -50, 3)$m, respectively, while the UEs are within a circle centered at $(70, 0, 2)$m. M ranges from 4 to 12. Set $N_t = 4$, $N = 64$, $\mathrm{P}_{\max} = 0.02$W, $\sigma^2 = -80$dBm, and the bandwidth to 10 MHz. The path loss model is $L(d) = C_0 (d/d_0)^{\kappa}$, with $C_0 = -30$dB at $d_0 = 1$m and κ as the path loss exponent. Specific κ and small-scale fading parameters are from [7]. The AP-RIS link is LoS, while the AP-UE and RIS-UE links are NLoS.

The following algorithms are compared: the proposed Algorithm 1 (JPAPB+w); the proposed algorithm with GNN-LSTM and RIS (JPAPB+w+GNNLSTM); Scaling-based algorithm with RIS (JPAPB+w+Scaling); Bisection-based design with random RIS (JPAPB+rw); Bisection-based design without RIS (JPAPB+wo). Graph neural network-long short-term memory (GNN-LSTM) is designed for determining p_{mk}.

There are several observations from Fig. 2(a). First, it indicates that the data rate can benefit from the presence of RIS based on curves "JPAPB+w", "JPAPB+rw" and "JPAPB+wo". The reason is that RIS adds a signal for the servicing user in the system. Second, curve "JPAPB+w+scaling" exhibits an abnormally lower data rate than Curve "JPAPB+wo". The reason for this anomaly is that the algorithm scales the power allocation variable to meet power constraints, resulting in a greater performance loss than that caused by the absence of RIS. Third, the relative positions of UEs and the RIS affect the data rate performance of the whole system, since the UEs can receive strong signals reflected from the RIS. The proposed

algorithm obtains the highest data rate, among a host of comparative baselines. Fig. 2(b) evaluates the performance of the proposed algorithm with respect to the maximum transmit power per AP. Overall, the data rate of the system increases as the maximum transmit power increases. However, the increase in data rate slows down in the increasing process of $\mathrm{P}_{\max}$. What's more, the gap between the performance achieved by "scaling" and that achieved by "bisection" decreases with the increasing transmitting power because the error caused by the "scaling" operation becomes small with the increase in transmitting power.

Fig. 3(a) evaluates the impact of increasing the number of UEs in the CFN-RIS on the achievable data rate per UE. As the number of UEs grows, the performance gap between different algorithms narrows, and the benefits provided by the RIS diminish. This gain reduction is primarily due to the increased interference experienced by each UE. Fig. 3(b) depicts the relationship between data rate and fronthaul capacity C. As C increases, the weighted data rate of both schemes improves. When $C < 2.5$, regardless of the existence of RIS, the non-coherent scheme outperforms the coherent scheme. The reason is the limitation of the coherent scheme under low C, where APs must transmit identical signals to the same UE, limiting the UE's maximum data rate to $K \times C$. In contrast, in the non-coherent scheme, different APs within the same UE service group can transmit diverse signals, aggregating their rates at the UE, potentially reaching up to C. Fig. 3(b) also illustrates that under limited fronthaul capacity, the performance gains from RIS in coherent transmission are minimal. Although RIS has the potential to enhance system performance, the limitation imposed by fronthaul capacity reduces its benefits.

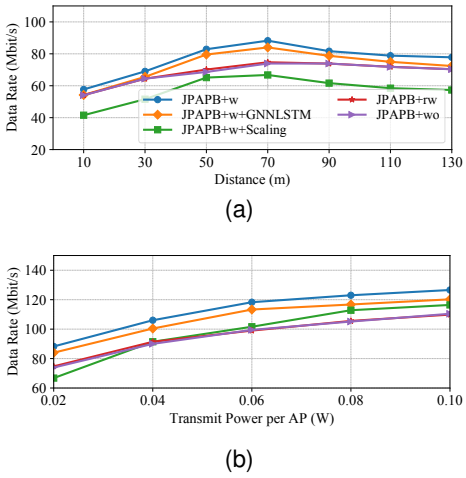

Fig. 2. Data rate against (a) distance of UE-RIS pairs. (b) transmitting powers.

VI. Conclusion

This letter analyzes the performance of RIS-CFN systems under two different transmission modes. The study demonstrates that coherent transmission is significantly affected by asynchronous reception and the fronthaul capacity limit. Then, we preferred non-coherent transmission and developed the JPAPA algorithm for non-coherent transmission, which jointly optimizes power allocation and phase to achieve higher data rates. Experimental results show that non-coherent transmission offers superior data rate performance under conditions of limited fronthaul capacity. In contrast, these capacity limitations reduce the gains from RIS in coherent transmission.

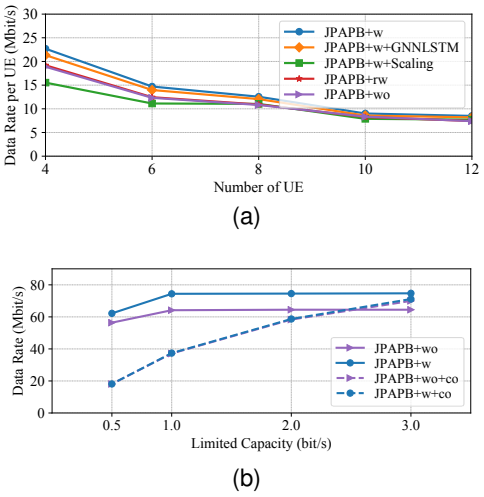

Fig. 3. Data rate against (a) numbers of UEs. (b) fronthaul capacity C.

References

[1] Q. Wu, S. Zhang, B. Zheng, C. You, and R. Zhang, "Intelligent reflecting surface-aided wireless communications: A tutorial," *IEEE Trans. Commun.*, vol. 69, no. 5, pp. 3313–3351, 2021.

[2] Z. Lin, H. Niu, K. An, Y. Wang, G. Zheng, S. Chatzinotas, and Y. Hu, "Refracting RIS-aided hybrid satellite-terrestrial relay networks: Joint beamforming design and optimization," *IEEE Trans. Aerosp. Electron. Syst.*, vol. 58, no. 4, pp. 3717–3724, 2022.

[3] K. An, Y. Sun, Z. Lin, Y. Zhu, W. Ni, N. Al-Dhahir, K.-K. Wong, and D. Niyato, "Exploiting multi-layer refracting RIS-assisted receiver for HAP-SWIPT networks," *IEEE Trans. Wireless Commun.*, 2024.

[4] A. Papazafeiropoulos, H. Q. Ngo, P. Kourtessis, and S. Chatzinotas, "STAR-RIS assisted cell-free massive MIMO system under spatially-correlated channels," *IEEE Trans. Veh. Technol.*, 2023.

[5] T. Van Chien, H. Q. Ngo, S. Chatzinotas, M. Di Renzo, and B. Ottersten, "Reconfigurable intelligent surface-assisted cell-free massive MIMO systems over spatially-correlated channels," *IEEE Trans. Wireless Commun.*, vol. 21, no. 7, pp. 5106–5128, 2021.

[6] E. Shi, J. Zhang, R. He, H. Jiao, Z. Wang, B. Ai, and D. W. K. Ng, "Spatially correlated reconfigurable intelligent surfaces-aided cell-free massive MIMO systems," *IEEE Trans. Veh. Technol.*, vol. 71, no. 8, pp. 9073–9077, 2022.

[7] Z. Zhang and L. Dai, "A joint precoding framework for wideband reconfigurable intelligent surface-aided cell-free network," *IEEE Trans. Signal Process.*, vol. 69, pp. 4085–4101, 2021.

[8] J. Zheng, J. Zhang, J. Cheng, V. C. Leung, D. W. K. Ng, and B. Ai, "Asynchronous cell-free massive MIMO with rate-splitting," *IEEE J. Sel. Areas Commun.*, vol. 41, no. 5, pp. 1366–1382, 2023.

[9] J. Li, M. Liu, P. Zhu, D. Wang, and X. You, "Impacts of asynchronous reception on cell-free distributed massive MIMO systems," *IEEE IEEE Trans. Veh. Technol.*, vol. 70, no. 10, pp. 11 106–11 110, 2021.

[10] X. Yan, Z. Wang, Y. Jia, Z. Zhang, and Y. Huang, "Access point selection and beamforming design for cell-free network: From fractional programming to GNN," *IEEE Trans. Wireless Commun.*, 2024.

[11] R. P. Antonioli, I. M. Braga, G. Fodor, Y. C. Silva, A. L. de Almeida, and W. C. Freitas, "On the energy efficiency of cell-free systems with limited fronthauls: Is coherent transmission always the best alternative?" *IEEE Trans. Wireless Commun.*, vol. 21, no. 10, pp. 8729–8743, 2022.

[12] C. Pan, H. Ren, M. Elkashlan, A. Nallanathan, and L. Hanzo, "The non-coherent ultra-dense c-RAN is capable of outperforming its coherent counterpart at a limited fronthaul capacity," *IEEE J. Sel. Areas Commun.*, vol. 36, no. 11, pp. 2549–2560, 2018.

[13] K. Shen and W. Yu, "Fractional programming for communication systems—part I: Power control and beamforming," *IEEE Trans. Signal Process.*, vol. 66, no. 10, pp. 2616–2630, 2018.